Journal of Optics

PAPER

OAM-mode sorting with a wavefront twister: a proposal

IOP Publishing J. Opt. 28 (2026) 085202 https://doi.org/10.1088/2040-8986/ae988d

Journal of Optics

RECEIVED
24 April 2026

REVISED
7 August 2026

ACCEPTED FOR PUBLICATION
12 August 2026

PUBLISHED
25 August 2026

PAPER

OAM-mode sorting with a wavefront twister: a proposal

Suman Karan[1,3], **Swati Chaudhary**[2,3], **Harshawardhan Wanare**[1] **and Anand K Jha**[1,*]

[1] Department of Physics, Indian Institute of Technology Kanpur, Kanpur, UP 208016, India
[2] The Institute for Solid State Physics, The University of Tokyo, Kashiwa, Chiba, Japan
[3] These authors contributed equally to this work.
[*] Author to whom any correspondence should be addressed.

E-mail: akjha@iitk.ac.in

Keywords: orbital angular momentum, OAM mode sorting, wavefront twister, wavefront rotator, Laguerre–Gaussian modes, high-dimensional quantum information, quantum key distribution

Abstract

We propose an orbital angular momentum (OAM) sorter based on a novel optical element that we refer to as a wavefront twister. It is a generalization of conventional wavefront rotators, such as the Dove prism. However, unlike a Dove prism, which simply rotates a wavefront, the rotation generated by a wavefront twister varies linearly with radial position. This variation results in the twisting of the outgoing wavefront, characterized by the twisting parameter a. We numerically demonstrate that the wavefront twister, followed by a lens, maps an OAM mode of index $|l|$ to an annulus at the back focal plane of the lens. We show that the transverse shape and size of the annulus depend on the radial field profile of the OAM mode, whereas its mean radial position is determined by $|l|$ and the twisting parameter a. Thus, OAM modes can be sorted with negligible intermodal overlap by appropriately adjusting the twisting parameter a. This proposal offers a scalable scheme for high-dimensional OAM mode sorting, with important consequences for the practical realization of OAM-based applications.

1. Introduction

Light beams can carry both spin and orbital angular momentum (OAM), associated with circular polarization and helical wavefront respectively [1]. Laguerre–Gaussian (LG) beams $LG_p^l(\rho,\phi)$ within the paraxial approximation carry a well-defined OAM of $l\hbar$ per photon, where l is an unbounded integer characterizing the azimuthal phase dependence of the form $e^{il\phi}$ [1], and p is the radial mode index characterizing the radial profile. Unlike polarization degree of freedom which is limited to two dimensions, the unbounded nature of l makes LG modes a natural high-dimensional basis. Furthermore, Mair *et al* [2] demonstrated that OAM of photon pairs generated in spontaneous parametric down-conversion is entangled, showing that LG modes can serve as a high-dimensional basis in quantum domain as well. These properties of OAM have led to a wide range of both classical and quantum information applications including high-capacity optical communication through free-space [3] and optical fibre [4], quantum key distribution [5, 6], quantum gate implementations [7, 8], supersensitive angular measurements [9], and for fundamental tests of quantum mechanics [10, 11].

Harnessing the full capacity of OAM in these applications requires not just detecting OAM modes but sorting them. An OAM detector measures the modal probability distribution [2, 12–14]. However, a sorter maps each mode to a distinct spatial location, enabling parallel detection, multiplexing, and mode-selective operations. For example, a prism spatially separates different frequency components. A lens maps different transverse wavevectors to distinct positions in the focal plane. A device that performs the analogous operation for OAM modes, an OAM sorter, remains a longstanding challenge.

Existing OAM sorting approaches include interferometric methods based on cascaded Mach–Zehnder interferometers with Dove prisms [12, 15], which are in principle 100% efficient but require $N-1$ interferometers to sort N modes, making them impractical for large mode sets. Log-polar coordinate transformation based sorters were first demonstrated by Berkhout *et al* [16] using two planar phase elements, sorting up to $l = \pm 5$ but with approximately 70% diffraction loss due to the limited efficiency of the SLM. Lavery *et al* [17, 18] later improved this efficiency using custom refractive elements, reducing loss to $\approx 15\%$ and extending the range to $l = \pm 25$ at the single-photon level. However, these sorters convert OAM modes into rectangular stripes, wash out the azimuthal phase, and suffer from around 20% crosstalk between consecutive OAM modes due to the finite size of the transformed beam. Mirhosseini *et al* [19] reduced this crosstalk to 2.6% by incorporating an additional refractive beam-copying element with log-polar transformation [20]. Although the inverse of the log-polar transformation has been demonstrated for OAM multiplexing [21], it has not been demonstrated for the modified technique by Mirhosseini *et al* [19]. In a different approach, the angular lens proposed by Sahu *et al* [22] sorts OAM modes into localized spots at separated angular positions using a single phase-only element. However, for experimentally feasible aperture sizes the sorting is possible with a minimum mode separation $\Delta l = \pm 3$. This sorter has also been demonstrated using metamaterials [23]. More recently, a multi-plane light conversion based LG mode sorter has been proposed, but it requires spatially separated input modes to begin with, limiting its applicability as an OAM sorter [24].

Thus, efficient and unambiguous OAM sorting is still an open challenge. To this end, in this article, we propose a novel optical element, which we refer to as a 'wavefront twister.' Based on this element, we demonstrate an OAM sorting scheme that ensures negligible intermodal overlap, preserves the circular symmetry of each mode, and is scalable to an arbitrarily large OAM mode set.

2. Proposed scheme

The concept of a wavefront twister

Figure 1(a) illustrates the action of a conventional wavefront rotators such as the Dove prism. A wavefront rotator oriented at angle θ_0 rotates an incoming wavefront by an angle $2\theta_0$. The rotation thus generated does not depend on the details of incoming wavefront. Therefore, in terms of cylindrical coordinates (ρ, ϕ, z), a wavefront rotator maps a point (ρ, ϕ) in the incoming wavefront to the point $(\rho, \phi + 2\theta_0)$ in the outgoing wavefront. In this work, we propose a wavefront twister by generalizing the idea of wavefront rotation. Unlike a wavefront rotator, which simply rotates a wavefront, the rotation generated by a wavefront twister varies linearly with radial position, resulting in the twisting of the incoming wavefront as illustrated in figures 1(b) and (c). The rotation $\theta(\rho)$ experienced by the incoming wavefront thus depends on the radial position and can be expressed as $\theta(\rho) = a\rho$, where a characterizes the strength of the twisting, and we refer to it as the twisting parameter. In terms of the cylindrical coordinates, the action of a wavefront twister is to map a point (ρ, ϕ) in the incoming wavefront to the point $(\rho, \phi + a\rho)$ in the outgoing wavefront, as shown in figure 1(c).

The action of a wavefront twister on an LG mode

For LG beams with radial index $p = 0$, the incident electric field profile at $z = 0$ is given by

$$E_l^{\mathrm{LG}}(\rho, \phi; z = 0) \equiv E_l^{\mathrm{LG}}(\rho, \phi) = E_l^{\mathrm{LG}}(\rho)\,\mathrm{e}^{-\mathrm{i}l\phi} \sqrt{\frac{2}{\pi w_0^2 |l|!}} \left(\frac{\sqrt{2}\rho}{w_0}\right)^{|l|} \mathrm{e}^{-\frac{\rho^2}{w_0^2}}\,\mathrm{e}^{-\mathrm{i}l\phi}, \tag{1}$$

where w_0 is the beam waist of the mode and l is the OAM mode index. While most OAM sources use LG modes with $p = 0$, OAM entangled states generated from spontaneous parametric down-conversion for a given l can have contributions from various p modes, including $p = 0$ [25, 26]. The generalization of our calculation to LG mode with $p \neq 0$ is discussed in appendix B. Since a wavefront rotator oriented at angle θ_0 rotates an incoming wavefront by $2\theta_0$, an incoming LG mode $E_l^{\mathrm{LG}}(\rho, \phi)$ given by equation (1) upon passing through an image rotator gets transformed as

$$E_l^{\mathrm{LG}}(\rho)\,\mathrm{e}^{-\mathrm{i}l\phi} \rightarrow E_l^{\mathrm{LG}}(\rho)\,\mathrm{e}^{-\mathrm{i}l(\phi + 2\theta_0)}. \tag{2}$$

We note that the action of a wavefront rotator on an LG mode of OAM mode index l can be modelled as a linear transformation in which the mode acquires a phase term $\mathrm{e}^{-\mathrm{i}l2\theta_0}$. In an analogous manner, since the rotation experienced by an incoming wavefront passing through a wavefront twister is given by $\theta(\rho) = a\rho$, the effect of a wavefront twister on an LG mode can be modelled as a linear transformation

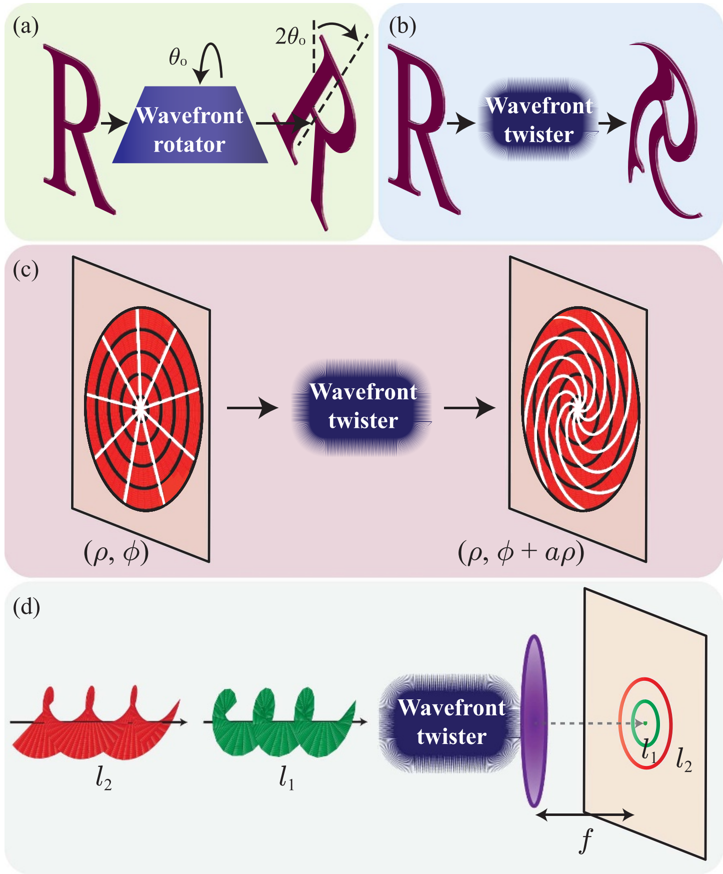

Figure 1. Conceptual illustration of the proposed wavefront twister and the OAM sorting scheme. (a) A conventional wavefront rotator such as a Dove prism, oriented at angle θ_0 rotates an input wavefront by angle $2\theta_0$. (b) The proposed wavefront twister rotates an incoming wavefront by an angle $\theta(\rho) = a\rho$ that varies linearly with radial location ρ. Consequently, the wavefront is not simply rotated but twisted. (c) The wavefront twister maps the point (ρ, ϕ) in the incident wavefront to $(\rho, \phi + a\rho)$. (d) The proposed OAM sorter scheme consisting of the wavefront twister followed by a lens of focal length f maps the OAM modes l_1 and l_2 to annuli of distinct radii in the focal plane, leading to their spatial separation.

in which the mode acquires a phase term $\mathrm{e}^{-ila\rho}$. This can be expressed as

$$E_l^{\mathrm{LG}}(\rho)\,\mathrm{e}^{-il\phi} \rightarrow E_l^{\mathrm{LG}}(\rho)\,\mathrm{e}^{-il(\phi+a\rho)}. \tag{3}$$

We note that the LG modes acquire l-dependent radial phase gradients upon passing through a wavefront twister. We show in the next subsection that this feature enables OAM-mode sorting with almost negligible intermodal overlap.

OAM-mode sorting with a wavefront twister

Our proposed scheme for OAM-mode sorting is shown in figure 1(d). A convex lens of focal length f is placed immediately after a wavefront twister and the resulting field distribution is measured at a screen placed at the back focal plane of the lens. For an incident LG mode field, the electric field at the lens, as shown in figure 1(d), is given by $E_l^{\mathrm{LG}}(\rho,\phi)\mathrm{e}^{-ila\rho}$ (equation (3)). Using the Fresnel–Kirchhoff diffraction integral, the electric field at a distance z from the lens, $E(r,\theta;z)$ can be written as:

$$E(r,\theta;z) = A(k,z)\int_0^{\infty}\int_0^{2\pi} E_l^{\mathrm{LG}}(\rho,\phi)\,\mathrm{e}^{-ila\rho}\mathrm{e}^{-\mathrm{i}\frac{k}{2f}\rho^2}\mathrm{e}^{\mathrm{i}\frac{k}{2z}\left[r^2-2r\rho\cos(\phi-\theta)+\rho^2\right]}\rho\,\mathrm{d}\rho\,\mathrm{d}\phi. \tag{4}$$

Here, (r,θ) represents the cylindrical coordinates at z. At $z = f$, the above equation reduces to

$$E(r,\theta,f) = A(k,z)\,\mathrm{e}^{\mathrm{i}\frac{k}{2f}r^2}\int_0^{\infty}\int_0^{2\pi} E_l^{\mathrm{LG}}(\rho,\phi)\,\mathrm{e}^{-ila\rho}\mathrm{e}^{-\mathrm{i}\frac{kr\rho}{f}\cos(\phi-\theta)}\rho\,\mathrm{d}\rho\,\mathrm{d}\phi. \tag{5}$$

Substituting from equation (1) and using the identity $e^{-i\frac{kr\rho}{f}\cos(\phi-\theta)} = \sum_n (-i)^n J_n\left(\frac{kr\rho}{f}\right) e^{-in\theta} e^{in\phi}$, equation (5) reduces to a one-dimensional integral:

$$E(r,\theta,f) = 2\pi\sqrt{\frac{2}{\pi w_0^2|l|!}}(-i)^l A(k,z)\, e^{i\frac{k}{2f}r^2} e^{-il\theta}\int_0^\infty e^{-\frac{\rho^2}{w_0^2}} e^{-ila\rho} J_l\left(\frac{kr\rho}{f}\right)\left(\frac{\sqrt{2}\rho}{w_0}\right)^{|l|}\rho\,\mathrm{d}\rho, \tag{6}$$

which can also be evaluated as an infinite summation of hypergeometric functions (see appendix A for a detailed derivation). We numerically compute $I_l(r) \equiv |E(r,\theta,z=f)|^2$ from the integral in equation (6) for different OAM mode index l and plot the results in figures 2. We quantify the overlap between adjacent OAM modes l and $l+1$ as the overlap area between their normalized radial intensity profiles, $I_l(r)$ and $I_{l+1}(r)$. We refer to it as the intermodal overlap C and define it as

$$C = \frac{\int \min\{I_l(r), I_{l+1}(r)\}\,\mathrm{d}r}{\int \max\{I_l(r), I_{l+1}(r)\}\,\mathrm{d}r} \times 100\%. \tag{7}$$

Here, $\min\{I_l(r), I_{l+1}(r)\}$ and $\max\{I_l(r), I_{l+1}(r)\}$ represent the minimum and the maximum of the two intensity values $I_l(r)$ and $I_{l+1}(r)$ at a given r. $C = 100\%$ represents complete overlap between the adjacent modes while $C = 0\%$ represents no intermodal overlap and hence perfect sorting of modes. If each mode is assigned an annular detection bin based on its radial position, C is directly related to the fraction of the intensity of one mode that is collected in the neighbouring mode"s detection bin, that is, the crosstalk in the conventional sense used in the sorter literature [19, 22]. A negligible C therefore corresponds to negligible crosstalk between adjacent OAM channels.

3. Results

Figure 2 shows the numerically computed intensities at the back focal plane of the lens for different $|l|$ values at various values of a, w_0, and p. In figure 2, the left column of sub-figures figures 2(a)–(g) plot the two-dimensional intensity profiles $|E(r,\theta,f=200\text{ mm})|^2$ while the right column of sub-figures figures 2(b), (d), (f) and (h) plot the one-dimensional intensity profiles $|E(r,\theta=0,f=200\text{ mm})|^2$ as a function of r. Figures 2(a) and (b) are the numerical plots at $a=\pi$ mm^{-1} and $w_0 = 1$ mm, and $p = 0$. We see that with this set of parameters, the modes are not completely sorted since the inter modal overlap $C = 15.45\%$. However, increasing the twisting parameter from $a = \pi$ mm^{-1} to $a = 3\pi$ mm^{-1} results in perfect sorting, as shown in figures 2(c) and (d), which are the numerical plots at $a = 3\pi$ mm^{-1} and $w_0 = 1$ mm, and $p = 0$. The intermodal overlap in this case is only about 0.05%, implying perfect sorting of OAM modes.

We next illustrate how the twisting parameter a affects sorting of modes. To this end, we note that the radial intensity profiles of the modes in figures 2(b) and (d), which are in the form of an annulus, can be well approximated by Gaussian functions. We refer to the mean and the standard deviation of the Gaussian function as the mean radial position μ and width of the annulus σ corresponding to a given mode $|l|$. In figures 3(a) and (b), we plot the mean radial position μ and width σ as a function of l for $a = \pi$ mm^{-1} and $a = 3\pi$ mm^{-1} for $w_0 = 1$ mm and $p = 0$. Figure 3(c) plots the intermodal overlap C as function of a at $w_0 = 1$ mm and $p = 0$. We note that the mean radial position of the annulus increases linearly with l and that the separation between consecutive annuli increases with a. On the other hand, the width σ of the modes remains almost independent of $|l|$ and a. Furthermore, we note that the intermodal overlap C decreases as a is increased. Thus, for a given set of $|l|$ modes, defined by the beam waist w_0 and the radial index p, one can find an optimum a such that the modes are completely sorted, that is, C approaches 0.

Next, we investigate how this sorter works for a set of $|l|$ with varying radial profile. To this end, we consider two sets of $|l|$ modes. For each set of modes, we choose a such that the intermodal overlap is less than 0.1%. For the first set of modes, we take $w_0 = 0.5$ mm and $p = 0$ and plot the corresponding numerical results in figures 2(e) and (f). For the second set, we take $w_0 = 1$ mm and $p = 1$ and plot the corresponding numerical results in figures 2(g) and (h). The detailed calculations for $p \neq 0$ mode is presented in appendix B. We see that since the $|l|$ modes in this case are radially structured, the radial profile of the annulus also become structured and as a result wider. As noted above, the mean radial position of an $|l|$ mode is decided by the twisting parameter a. However, as we see from figures 2(e) and (h), the transverse shape and size of the annulus at the back focal plane is affected by the radial field profile of the modes, that is by the beam waist w_0 and the radial mode index p. Thus although the radial field

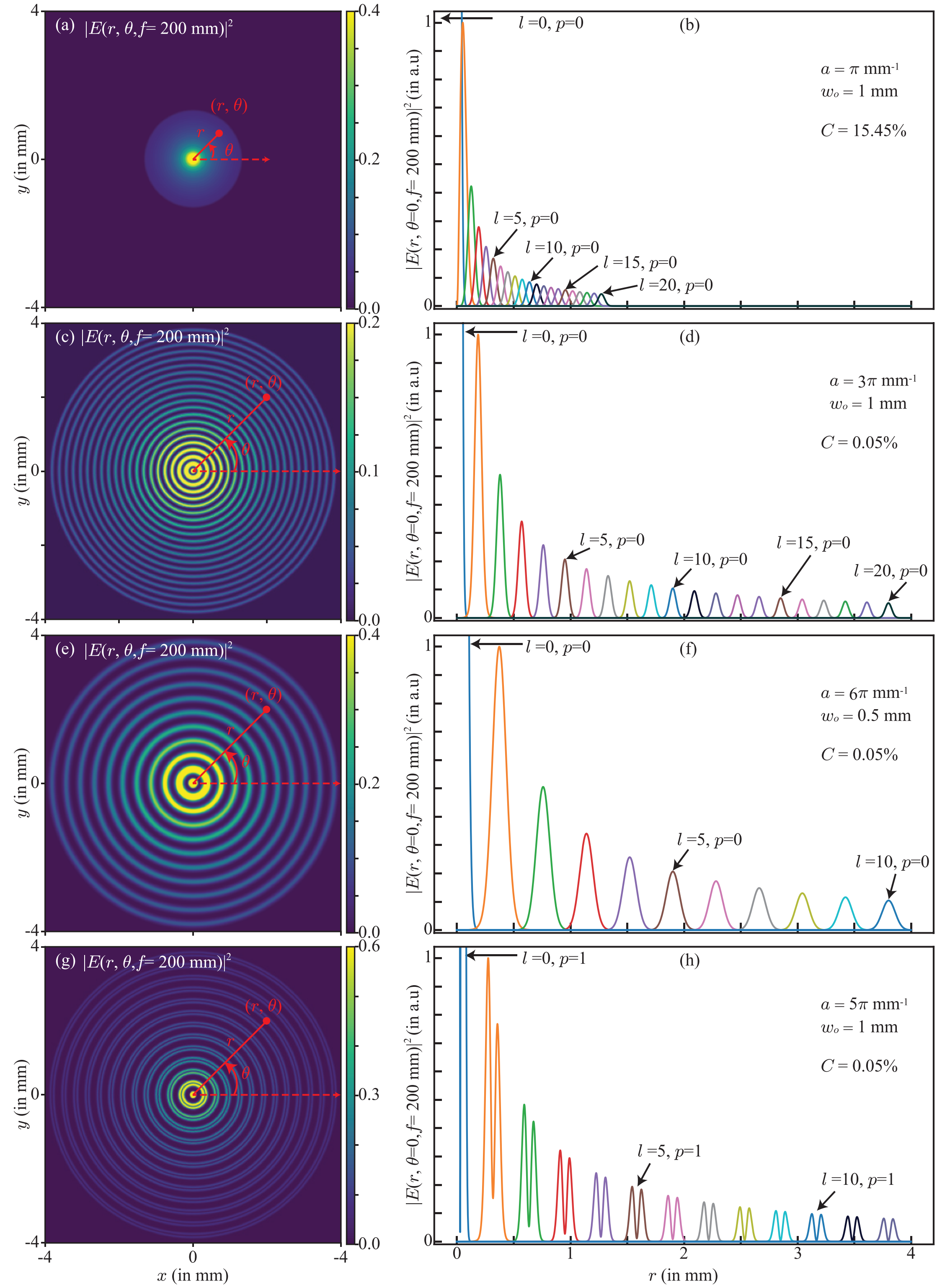

Figure 2. Plots of numerically computed two-dimensional intensity $|E(r, \theta, f = 200\text{ mm})|^2$ as a function of (x, y) and numerically computed one-dimensional intensity profiles $|E(r, \theta = 0, f = 200\text{ mm})|^2$ as a function of r, for OAM mode index l ranging from 1 to 20. (a) and (b) $a = \pi$ mm^{-1}, $w_0 = 1$ mm, $p = 0$. (c) and (d) $a = 3\pi$ mm^{-1}, $w_0 = 1$ mm, $p = 0$. (e) and (f) $a = 6\pi$ mm^{-1}, $w_0 = 0.5$ mm, $p = 0$. (g) and (h) $a = 5\pi$ mm^{-1}, $w_0 = 1$ mm, $p = 1$.

profile of the incoming $|l|$ modes does affect the intermodal overlap C, its effect can be countered by appropriately choosing the twisting parameter a such that the intermodal overlap C is negligible.

We note that our sorting scheme works not only for a given beam waist w_0 or the radial mode index p but also for varying values of these parameters or even when the radial field profile is structured, which can be generated by taking $p \neq 0$ modes or a superposition of p modes. Finally, we note that, this sorting scheme in principle can sort an arbitrarily large number of modes with the same efficiency.

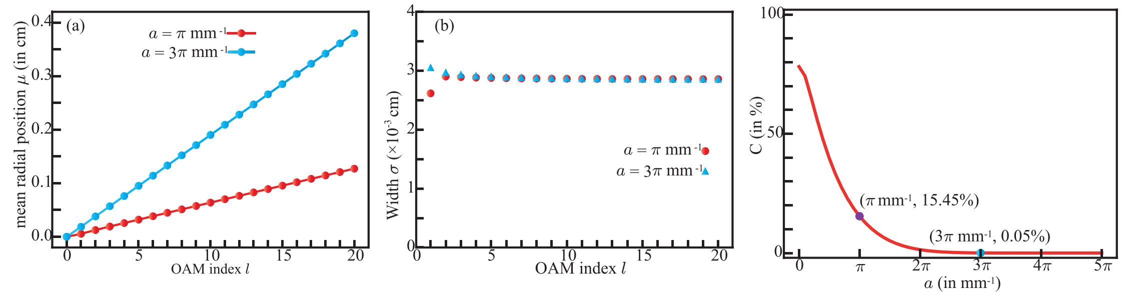

Figure 3. (a) Plot of the mean radial position μ of the annuli shown in figures 2(a) and (c) as a function of l. (b) Plot of the width μ of the annuli shown in figures 2(a) and (c) as a function of l. (c) The intermodal overlap C as a function of a, for $w_0 = 1$ mm and $p = 0$. We see that the intermodal overlap decreases monotonically with increasing a. The two highlighted points correspond to $a = \pi$ mm^{-1} and 3π mm^{-1}.

However, the upper bound on the number of modes that can be sorted depends on the size and the twisting parameter of the wavefront twister, the lens aperture, and the size of the detector at the back focal plane.

4. Conclusions and discussion

In summary, we have proposed a wavefront twister, an optical element that twists an incoming wavefront such that the rotation experienced by the wavefront varies linearly with radial position. Utilizing this optical element, we have demonstrated an OAM-mode sorting scheme in which an OAM mode of index $|l|$ is mapped to an annulus at the back focal plane of a lens. The transverse shape and size of the annulus depend on the radial field profile of the $|l|$ mode, while its mean radial position is determined by $|l|$ and the twisting parameter a. We have shown that the twister can sort OAM modes of different beam waists w_0 as well as different radial mode indices p. In general, the sorter distinguishes the modes based on their $|l|$ value. The radial field profile of the incoming mode determines the shape and size of the annulus at the back focal plane of the lens. Because the mean radial position of the annulus depends on the twisting parameter a, one can always choose a twisting strength a that is sufficient to sort the given OAM modes. Therefore, the experimental realization of a wavefront twister could have several important consequences for the practical implementation of OAM-based quantum and classical communication schemes.

We note that the coordinate transformation $(\rho,\phi) \rightarrow (\rho,\phi + a\rho)$ underlying the proposed twister cannot, in general, be implemented by a single phase element. This is true even for realizing a conventional wavefront rotator in the form of a Dove prism or K-mirror system, which requires three distinct planar phase elements, including one out-of-plane reflector. One possible implementation of the twister is to realize a radially segmented image rotator in which wavefront rotation is achieved within discrete radial segments, with the rotation of successive radial segments progressively increasing. This segmentation can be achieved by using two radially segmented lenses that tilt different annular portions of an incoming wavefront at different azimuthal locations within the focal plane. The two lenses are arranged in a 4f configuration. The first lens focuses the wavefront segment-wise; the light is then reflected and recombined at the second radially segmented lens, which converts each segment back into the original wavefront, but with each segment rotated by a different angle. We further note that, in our proposed sorting scheme, the mean radial position of the annulus at the back focal plane depends on the OAM mode's index $|l|$, and the sensitivity of sorting, which is quantified in terms of the intermodal overlap C, is determined by the twisting parameter. Therefore, our scheme is highly sensitive to changes in the $|l|$ mode spectrum and can, in principle, be used to detect such changes. For example, using this sorting scheme, a small misalignment of the modes with respect to the wavefront twister can be measured, since misalignment causes the $|l|$ spectrum to change [27]. Also, our proposed twister preserves the circular symmetry of the modes even after sorting. This is in contrast to log-polar-transformation-based implementations of an OAM sorter, in which circular symmetry is not maintained [16–19]. Finally, we note that our proposed sorter does not sort the sign of the OAM mode. However, it is known that an angular lens maps all OAM modes with a positive l index to the upper half-plane, while mapping all modes with a negative l index to the lower half-plane [22]. This property of an angular lens can in principle be combined with the sorting ability of the proposed twister to make a complete sorter that sorts even the helicity of the OAM modes.

Data availability statement

All data that support the findings of this study are included within the article (and any supplementary files).

Funding

We acknowledge financial support from the Science and Engineering Research Board through grants STR/2021/000 035 & CRG/2022/003 070, and from the Department of Science & Technology, Government of India through grant DST/ICPS/QuST/Theme-I/2019 and grant DST/FFT/NQM/QSM/2024/3 under the National Quantum Mission (NQM) Technical Group (TG) project on quantum imaging.

Appendix A. Field distribution in the back focal plane of the lens with the wavefront twister

We evaluate the radial integral in equation (6), which is given by

$$A_l(r) = \int_0^\infty \mathrm{e}^{-\frac{\rho^2}{w_0^2}} \mathrm{e}^{-\mathrm{i}la\rho} J_l\left(\frac{kr\rho}{f}\right)\left(\frac{\sqrt{2}\rho}{w_0}\right)^{|l|} \rho \mathrm{d}\rho. \tag{8}$$

To evaluate this integral, we first expand $\mathrm{e}^{-\mathrm{i}la\rho}$ as a power series of the form

$$\mathrm{e}^{-\mathrm{i}la\rho} = \sum_{m=0}^{\infty} \frac{(-\mathrm{i}la\rho)^m}{m!} = \sum_{m=0}^{\infty} \frac{(-\mathrm{i}la)^m}{m!}\rho^m. \tag{9}$$

Next, substituting this expansion and using the identity $J_l\left(\frac{kr\rho}{f}\right) = (-1)^{\frac{|l|-l}{2}} J_{|l|}\left(\frac{kr\rho}{f}\right)$ in equation (8), we get

$$A_l(r) = \sum_{m=0}^{\infty} \frac{(-\mathrm{i}la)^m}{m!}\left(\frac{\sqrt{2}}{w_0}\right)^{|l|}(-1)^{\frac{|l|-l}{2}} \int_0^\infty \mathrm{e}^{-\frac{\rho^2}{w_0^2}} J_{|l|}\left(\frac{kr\rho}{f}\right)\rho^{|l|+m+1}\mathrm{d}\rho. \tag{10}$$

The integral in each term of the summation can be evaluated using the identity from Gradshteyn & Ryzhik (6.631-1) [28]:

$$\int_0^\infty x^\mu \mathrm{e}^{-\alpha x^2} J_\nu(\beta x)\,\mathrm{d}x = \frac{\beta^\nu \Gamma\left(\frac{\nu+\mu+1}{2}\right)}{2^{\nu+1}\alpha^{\frac{\nu+\mu+1}{2}}\Gamma(\nu+1)}\, {}_1F_1\left[\frac{\nu+\mu+1}{2};\nu+1;-\frac{\beta^2}{4\alpha}\right]. \tag{11}$$

Setting $\alpha = 1/w_0^2$, $\mu = |l|+m+1$, $\nu = |l|$, and $\beta = kr/f$ in the above identity, equation (10) reduces to

$$A_l(r) = \sum_{m=0}^{\infty} \frac{(-\mathrm{i}la)^m}{m!}\left(\frac{\sqrt{2}kr}{w_0 f}\right)^{|l|}(-1)^{\frac{|l|-l}{2}} \frac{\Gamma\left(|l|+1+\frac{m}{2}\right)\left(w_0^2\right)^{|l|+1+\frac{m}{2}}}{2^{|l|+1}\Gamma(|l|+1)}$$
$$\times\, {}_1F_1\left[|l|+1+\frac{m}{2};|l|+1;-\frac{k^2r^2w_0^2}{4f^2}\right]. \tag{12}$$

$A_l(r)$ is thus an infinite summation of hypergeometric functions ${}_1F_1$. We evaluate the integral in equation (6) numerically.

Appendix B. Generalization to LG modes with $p \neq 0$

For a LG mode with radial index $p \neq 0$, the incident electric field profile at $z = 0$ is given by

$$E^{\mathrm{LG}}_{l,p}(\rho,\phi) = E^{\mathrm{LG}}_{l,p}(\rho)\,\mathrm{e}^{-il\phi} = \sqrt{\frac{2p!}{\pi w_0^2 (p+|l|)!}} \left(\frac{\sqrt{2}\rho}{w_0}\right)^{|l|} L_p^{|l|}\left(\frac{2\rho^2}{w_0^2}\right)\mathrm{e}^{-\frac{\rho^2}{w_0^2}}\,\mathrm{e}^{-\mathrm{i}l\phi}, \tag{13}$$

where $L_p^{|l|}$ is the associated Laguerre polynomial. For $p = 0$, $L_0^{|l|} = 1$ and equation (13) reduces to equation (1). Following the same procedure as in the main text, the action of the wavefront twister on this mode gives

$$E^{\mathrm{LG}}_{l,p}(\rho)\,\mathrm{e}^{-\mathrm{i}l\phi} \rightarrow E^{\mathrm{LG}}_{l,p}(\rho)\,\mathrm{e}^{-\mathrm{i}l(\phi+a\rho)}, \tag{14}$$

since the phase $\mathrm{e}^{-\mathrm{i}la\rho}$ depends only on the azimuthal index l and not on the radial index p. Therefore, substituting equation (13) in equation (5) and using the identity $\mathrm{e}^{-\mathrm{i}\frac{kr\rho}{f}\cos(\phi-\theta)} = \sum_n (-\mathrm{i})^n J_n\left(\frac{kr\rho}{f}\right)\mathrm{e}^{-\mathrm{i}n\theta}\mathrm{e}^{\mathrm{i}n\phi}$, the electric field at the back focal plane of the lens can be expressed as

$$E(r,\theta,f) = 2\pi(-\mathrm{i})^l A(k,z)\,\mathrm{e}^{\mathrm{i}\frac{k}{2f}r^2}\mathrm{e}^{-\mathrm{i}l\theta}\int_0^\infty E^{\mathrm{LG}}_{l,p}(\rho)\,\mathrm{e}^{-\mathrm{i}la\rho}J_l\left(\frac{kr\rho}{f}\right)\rho\mathrm{d}\rho, \tag{15}$$

$$= 2\pi\sqrt{\frac{2p!}{\pi w_0^2(p+|l|)!}}(-\mathrm{i})^l A(k,z)\,\mathrm{e}^{\mathrm{i}\frac{k}{2f}r^2}\mathrm{e}^{-\mathrm{i}l\theta} \times \int_0^\infty \mathrm{e}^{-\frac{\rho^2}{w_0^2}} L_p^{|l|}\left(\frac{2\rho^2}{w_0^2}\right)\mathrm{e}^{-\mathrm{i}la\rho}J_l\left(\frac{kr\rho}{f}\right)\left(\frac{\sqrt{2}\rho}{w_0}\right)^{|l|}\rho\mathrm{d}\rho, \tag{16}$$

where for $p = 0$ equation (16) reduces to equation (6) of the main text.

ORCID iDs

Suman Karan 0000-0003-0301-0020
Swati Chaudhary 0009-0007-2457-2950
Harshawardhan Wanare 0000-0003-3461-0336
Anand K Jha 0000-0002-5186-6264

References

[1] Allen L, Beijersbergen M W, Spreeuw R J C and Woerdman J P 1992 Orbital angular momentum of light and the transformation of Laguerre-Gaussian laser modes *Phys. Rev. A* **45** 8185–9
[2] Mair A, Vaziri A, Weihs G and Zeilinger A 2001 Entanglement of the orbital angular momentum states of photons *Nature* **412** 313–6
[3] Wang J *et al* 2012 Terabit free-space data transmission employing orbital angular momentum multiplexing *Nat. Photon.* **6** 488–96
[4] Bozinovic N *et al* 2013 Terabit-scale orbital angular momentum mode division multiplexing in fibers *Science* **340** 1545–8
[5] Cerf N J, Bourennane M, Karlsson A and Gisin N 2002 Security of quantum key distribution usingd-level systems *Phys. Rev. Lett.* **88** 127902
[6] Karimipour V, Bahraminasab A and Bagherinezhad S 2002 Quantum key distribution ford-level systems with generalized Bell states *Phys. Rev. A* **65** 052331
[7] Ralph T C, Resch K J and Gilchrist A 2007 Efficient Toffoli gates using qudits *Phys. Rev. A* **75** 022313
[8] Lanyon B P *et al* 2008 Simplifying quantum logic using higher-dimensional Hilbert spaces *Nat. Phys.* **5** 134–40
[9] Jha A K, Agarwal G S and Boyd R W 2011 Supersensitive measurement of angular displacements using entangled photons *Phys. Rev. A* **83** 053829
[10] Kaszlikowski D, Gnaciński P, Żukowski M, Miklaszewski W and Zeilinger A 2000 Violations of local realism by two entangledn-dimensional systems are stronger than for two qubits *Phys. Rev. Lett.* **85** 4418–21
[11] Collins D, Gisin N, Linden N, Massar S and Popescu S 2002 Bell inequalities for arbitrarily high-dimensional systems *Phys. Rev. Lett.* **88** 040404
[12] Leach J, Padgett M J, Barnett S M, Franke-Arnold S and Courtial J 2002 Measuring the orbital angular momentum of a single photon *Phys. Rev. Lett.* **88** 257901
[13] Kulkarni G, Sahu R, Magaña-Loaiza O S, Boyd R W and Jha A K 2017 Single-shot measurement of the orbital-angular-momentum spectrum of light *Nat. Commun.* **8** 1054
[14] Karan S, Van Exter M P and Jha A K 2025 Broadband uniform-efficiency OAM-mode detector *Sci. Adv.* **11** eadq7201
[15] Leach J, Courtial J, Skeldon K, Barnett S M, Franke-Arnold S and Padgett M J 2004 Interferometric methods to measure orbital and spin, or the total angular momentum of a single photon *Phys. Rev. Lett.* **92** 013601
[16] Berkhout G C G, Lavery M P J, Courtial J, Beijersbergen M W and Padgett M J 2010 Efficient sorting of orbital angular momentum states of light *Phys. Rev. Lett.* **105** 153601

[17] Lavery M P J, Robertson D J, Berkhout G C G, Love G D, Padgett M J and Courtial J 2012 Refractive elements for the measurement of the orbital angular momentum of a single photon *Opt. Express* **20** 2110

[18] Lavery M P J *et al* 2013 Efficient measurement of an optical orbital-angular-momentum spectrum comprising more than 50 states *New J. Phys.* **15** 013024

[19] Mirhosseini M, Malik M, Shi Z and Boyd R W 2013 Efficient separation of the orbital angular momentum eigenstates of light *Nat. Commun.* **4** 2781

[20] Malik M, Mirhosseini M, Lavery M P J, Leach J, Padgett M J and Boyd R W 2014 Direct measurement of a 27-dimensional orbital-angular-momentum state vector *Nat. Commun.* **5** 3115

[21] Huang H *et al* 2015 Mode division multiplexing using an orbital angular momentum mode sorter and MIMO-DSP over a graded-index few-mode optical fibre *Sci. Rep.* **5** 14931

[22] Sahu R, Chaudhary S, Khare K, Bhattacharya M, Wanare H and Jha A K 2018 Angular lens *Opt. Express* **26** 8709

[23] Guo Y *et al* 2021 Spin-decoupled metasurface for simultaneous detection of spin and orbital angular momenta via momentum transformation *Light: Sci. Appl.* **10** 63

[24] Fontaine N K, Ryf R, Chen H, Neilson D T, Kim K and Carpenter J 2019 Laguerre-Gaussian mode sorter *Nat. Commun.* **10** 1865

[25] Miatto F M, Yao A M and Barnett S M 2011 Full characterization of the quantum spiral bandwidth of entangled biphotons *Phys. Rev. A* **83** 033816

[26] Zhang Y, Roux F S, McLaren M and Forbes A 2014 Radial modal dependence of the azimuthal spectrum after parametric down-conversion *Phys. Rev. A* **89** 043820

[27] Vasnetsov M V, Pas'ko V A and Soskin M S 2005 Analysis of orbital angular momentum of a misaligned optical beam *New J. Phys.* **7** 46–46

[28] Gradshteyn I S and Ryzhik I M 2014 *table of Integrals, Series and Products* (Academic)